Cancer Research

Ovarian Cancers Harboring Inactivating Mutations in *CDK12* Display a Distinct Genomic Instability Pattern Characterized by Large Tandem Duplications

Tatiana Popova[1,2,3], Elodie Manié[1,2,3], Valentina Boeva[1,3,4], Aude Battistella[1,2,3], Oumou Goundiam[1,3,5,6,7], Nicholas K. Smith[1,2,3], Christopher R. Mueller[8], Virginie Raynal[1,2,3], Odette Mariani[3,6,9], Xavier Sastre-Garau[3,5,6], and Marc-Henri Stern[1,2,3]

Abstract

CDK12 is a recurrently mutated gene in serous ovarian carcinoma, whose downregulation is associated with impaired expression of DNA damage repair genes and subsequent hypersensitivity to DNA-damaging agents and PARP1/2 inhibitors. In this study, we investigated the genomic landscape associated with *CDK12* inactivation in patients with serous ovarian carcinoma. We show that *CDK12* loss was consistently associated with a particular genomic instability pattern characterized by hundreds of tandem duplications of up to 10 megabases (Mb) in size. Tandem duplications were characterized by a bimodal (~0.3 and ~3 Mb) size distribution and overlapping microhomology at the breakpoints. This genomic instability, denoted as the CDK12 TD-plus phenotype, is remarkably distinct from other alteration patterns described in breast and ovarian cancers. The CDK12 TD-plus phenotype was associated with a greater than 10% gain in genomic content and occurred at a 3% to 4% rate in The Cancer Genome Atlas–derived and in-house cohorts of patients with serous ovarian carcinoma. Moreover, *CDK12*-inactivating mutations together with the TD-plus phenotype were also observed in prostate cancers. Our finding provides new insight toward deciphering the function of CDK12 in genome maintenance and oncogenesis. *Cancer Res; 76(7); 1882–91. ©2016 AACR.*

Introduction

Cyclin-dependent kinase 12 (*CDK12*) as a tumor suppressor gene was discovered in The Cancer Genome Atlas (TCGA) study of high-grade serous ovarian carcinoma (HGS-OvCa; ref. 1). It appeared among the 10 most recurrently mutated genes in HGS-OvCa, which, besides *CDK12*, included *TP53*, *BRCA1*, *BRCA2*, *NF1*, and *RB1*. *CDK12* encodes a serine/threonine kinase involved in the regulation of RNA polymerase II (RNA pol II) and mRNA processing (2–4). CDK12 attracted particular attention as cells inactivated for the CDK12 display hypersensitivity to DNA-damaging agents and to PARP1/2 inhibitors (5, 6). This effect of *CDK12* inactivation was associated with homologous recombination (HR) deficiency (HRD) due to decreased expression observed for some HR genes, such as *BRCA1*, *FANCI*, or *FANCD2* (3, 5, 7, 8). HRD due to inactivation of *BRCA1* or *BRCA2*, the two major genes implicated in ovarian cancer, leads to the large-scale chromosomal instability, readily observed in nearly half of HGS-OvCa (9–11). The essential question is what type of genomic instability accompanies *CDK12* inactivation.

Here, we show that ovarian tumors inactivated for *CDK12* have a particular genomic instability with genomic profiles characterized by frequent mega-sized gains scattered over the genome, and this remarkable genomic architecture is due to numerous tandem duplications (TD).

Materials and Methods

Datasets of ovarian and breast carcinoma

TCGA cohorts. Controlled access data are from (i) serous ovarian carcinoma cohort (HGS-OvCa): 556 cases with SNP arrays including 527 cases with whole-exome sequencing (WES) or transcriptome (RNA-seq) sequencing data (1); (ii) breast carcinoma cohort: 760 cases with SNP arrays and WES/RNA-seq (12); (iii) prostate adenocarcinoma cohort: 407 cases with SNP arrays and WES/RNA-seq (12, 13). All human data were handled according to Data Access Request.

In-house cohort. Cohort includes 95 primary ovarian tumors of mainly serous subtype assembled in Institut Curie (14). According to French regulation, patients were informed of the research performed on tissue specimens and did not express opposition.

[1]Institut Curie, Centre de Recherche, Paris, France. [2]INSERM U830, Paris, France. [3]PSL Research University, Paris, France. [4]INSERM U900, Paris, France. [5]EA4340-BCOH, Versailles Saint-Quentin-en-Yvelines University, Guyancourt, France. [6]Institut Curie, Département de Biopathologie, Paris, France. [7]Institut Curie, Département de Recherche Translationnelle, Paris, France. [8]Queen's Cancer Research Institute, Queen's University, Kingston, Ontario, Canada. [9]Institut Curie, Centre de Ressources Biologiques, Paris, France.

Note: Supplementary data for this article are available at Cancer Research Online (http://cancerres.aacrjournals.org/).

The results presented here are in part based upon data generated by the TCGA Research Network: http://cancergenome.nih.gov/.

Corresponding Author: Tatiana Popova, Institut Curie, INSERM U830, 26 rue d'Ulm, 75248 Paris, France. Phone: 33156246517; Fax: 33156246630; E-mail: tatiana.popova@curie.fr

doi: 10.1158/0008-5472.CAN-15-2128

Data from public repositories. Data from public repositories include (i) GEO (GSE18461 and GSE29398) and Sequence Read Archive (SRA ERP000703 and ERP000704; ref. 15); and (ii) European Genome-phenome Archive (EGA; controlled access EGAS00001000155; ref. 16).

SKOV3 cell line. SKOV3 cell line obtained from the ATCC was verified by reference genomic and mutational profiles at the time of experiment. SNP array was obtained from the Cancer Cell Line Encyclopedia (17).

SNP-array processing

SNP arrays were normalized using ChAS, Genotyping Console, or Genome Studio software (18, 19). Absolute copy number and allelic contents were obtained using the Genome Alteration Print (GAP; ref. 20). DNA index was calculated as the averaged copy number. Tumor ploidy was set to 2 (near-diploid tumors) if DNA index <1.3 or to 4 (near-tetraploid tumors) if DNA index $\geq$1.3. Relative copy-number profile was calculated as ratio of copy-number/DNA index. The interstitial gains were calculated after filtering microalterations (<50 SNPs in size) and following a step-wise procedure starting with the smallest segments between two consecutive breakpoints. The number of large-scale state transitions (LST), representing the number of breakpoints between large chromosome fragments, was calculated as previously described (9).

Sequencing *CDK12* in tumor DNA and breakpoint validation

PCR and Sanger sequencing were performed using standard protocols available upon request.

Mate-pair whole genome sequencing

MP2, MP3, and MP4 primary ovarian tumors and the cell line SKOV3 were sequenced using whole genome sequencing (WGS) mate-pair technique on the platform sequencer Illumina HiSeq 2500 with read length of 100 $\times$ 100 bp and approximately 40$\times$ physical whole-genome coverage. Mate-pair library was constructed according to the manufacturer's protocol: fragmentation by Covaris (80 seconds), 30 mn Tagmentation, no size selection, and approximately 3,000 bp distance between mates.

WGS processing

Mate-pair WGS and paired-end WGS were aligned using Bfast and/or BWA 0.7.0a (21, 22) and processed using Samtools (23), BedTools (24), Picard tools (25), and Integrative Genomic Viewer (26), including SVdetect (27) and DELLY (28) for structural and Control-FREEC (29) for copy-number alterations, visualized by Circos (30). Breakpoint junctions were extracted from split-reads. Mutations were annotated by Annovar (31).

Analysis of gene expression

Analysis was performed on Affymetrix geneChip HG-U133A(B) and RNA-seq gene-level RPKM (reads per kilobase per million mapped reads). Expression data were obtained from public repositories (TCGA: https://tcga-data.nci.nih.gov/tcga and in-house: http://microarrays.curie.fr/publications/biopathology/ovarian_carcinoma; ref. 14). After preprocessing (Supplementary Methods), the reference subset of tumors was compiled from five nearest neighbors to each *CDK12*-mutated case detected in the subspace of five principal components, where principal component analysis was applied to the subgroup of non-*BRCA1/2* nonmesenchymal tumors.

Statistical analysis

Statistical analysis was performed using R (32).

Results

CDK12 inactivation is associated with a high frequency of interstitial gains

SNP-array analysis of 556 HGS-OvCa cases from the TCGA (1) showed a subset of 17 tumors with extremely altered genomes characterized by a high number of gains over the chromosome baseline (Fig. 1A). GAP patterns (a two-dimensional plot of segmental copy number and allelic difference values; ref. 20) ensured the consistency and excluded noise artifacts (Fig. 1B). Besides the overall high number of breakpoints in copy-number profiles, this group of tumors was found to be best characterized by the high number of interstitial gains of 2 to 7 megabases (Mb) in size (Fig. 1C and D). Inspection of WES and/or RNA-seq data showed that 15 of 17 tumors with the intensive gain pattern were mutated for *CDK12* (Table 1; Supplementary Fig. S1). *CDK12* mutations were deleterious (nonsense mutations or frameshifts due to indels, 9 cases; 1 splice) or with unknown consequences (3 missense mutations and 2 in-frame deletions in the kinase domain; Fig. 1E). All mutations were associated with LOH in the gene locus and showed prevailing allele frequency. As for the two remaining cases, one tumor was not found mutated in *CDK12* based on WES, and one tumor had no sequencing data. The mutational analysis of *CDK12* in tumors not displaying the intensive interstitial gain pattern (511 HGS-OvCa cases with sequencing data available) showed five missense mutations and three rare SNPs. Thus, there is a significant association between *CDK12* mutations and the highly altered genomes with intensive gain pattern (P value < 10^{-15}, Fisher test).

Quantitatively, tumors with frameshift and nonsense mutations in *CDK12* were characterized by more than 300 breakpoints (509 ± 72, median $\pm$ median absolute deviation) and more than 30 interstitial gains of 2 to 7 Mb (65 ± 12), which on average appeared to be 5 and 20 times more abundant compared with tumors not mutated for *CDK12* (104 ± 44 breakpoints and 3 ± 2 interstitial gains of 2 to 7 Mb, respectively). Missense mutations in *CDK12* that display the same phenotype as frameshift/nonsense mutations were further considered as deleterious (Table 1; Fig. 1E). Tumors with *CDK12* missense mutations and low rate of interstitial gains were classified as not bearing a genomic phenotype associated with *CDK12* inactivation, despite occasionally high level of genetic alterations (Supplementary Fig. S2). Importantly, the recently reported functional analysis of *CDK12* mutants (8), which included four of missense variants mentioned above, was concordant with our conclusion: two *CDK12* missense mutants not associated with an intensive regular gain pattern were shown to conserve their CCNK (cyclin K) interaction and/or kinase properties, whereas two *CDK12* missense mutants associated with such a genomic pattern were demonstrated to be pathogenic (Table 1).

For validation, in-house cohort of 95 ovarian carcinomas was investigated, and 4 tumors displaying a genome profile characterized by the high number of interstitial gains were detected. All these 4 tumors were found mutated for *CDK12* (three truncating mutations and one missense mutation in the protein kinase domain; all tumors displayed LOH in *CDK12* locus; Fig. 1D; Supplementary Fig. S3).

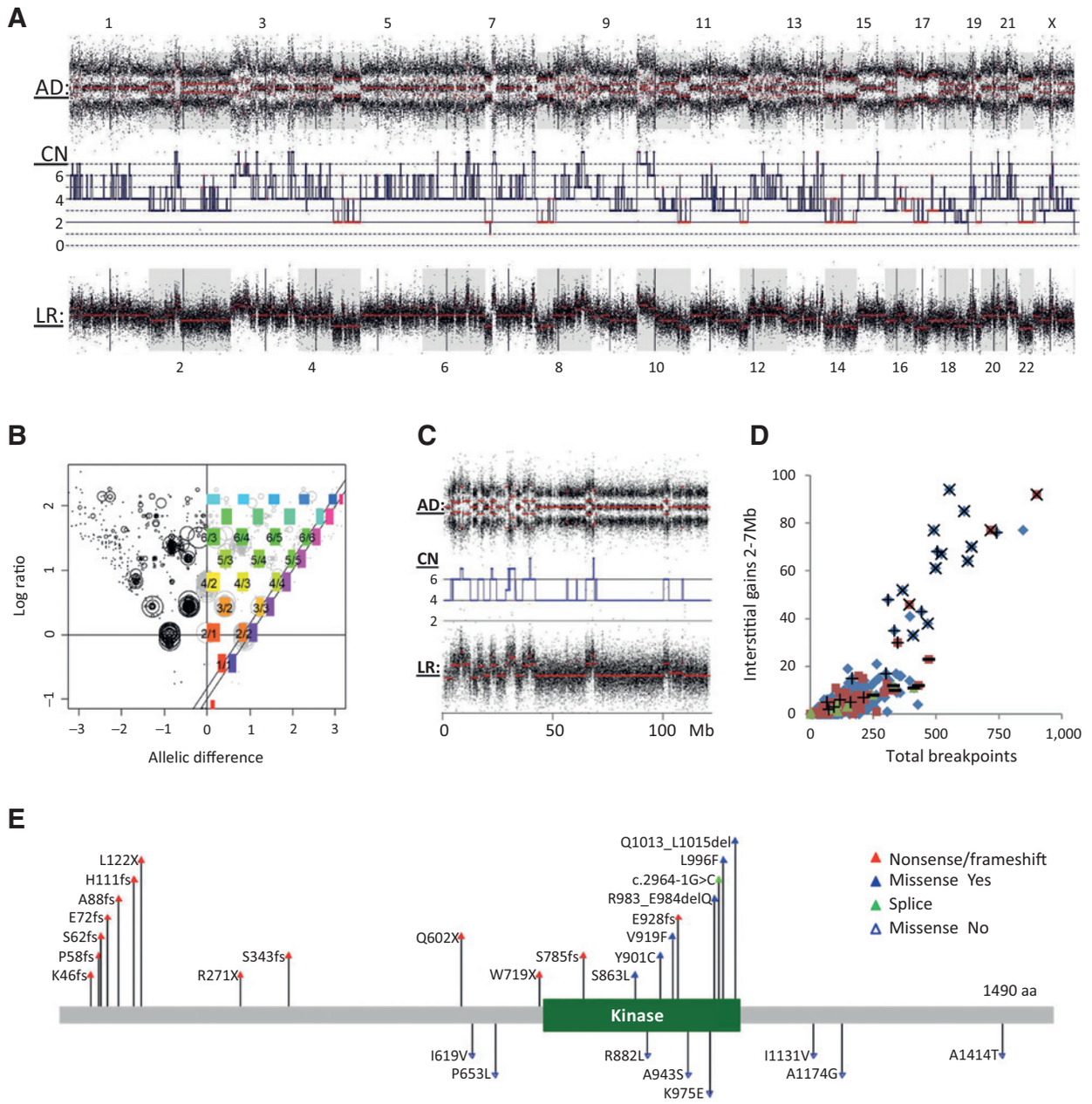

Figure 1.
Genomic phenotype of *CDK12*-mutated ovarian tumors. A, SNP-array profile of a *CDK12*-mutated tumor (CN, absolute copy number; LR, log R ratio; AD, allelic difference). B, GAP plot and copy-number recognition pattern of the SNP-array profile shown above; here, each circle corresponds to a genomic segment and the position of the circle is defined by LR (*y*-axis) and AD (*x*-axis). C, zoom-in on a fragment of the genomic profile. D, ovarian tumors characterized by the total number of breakpoints in the genomic profile (*x*-axis) and the number of interstitial gains of 2 to 7 Mb in size (*y*-axis) are shown, including TCGA (blue) and in-house (brown) cohorts and cases from ref. 15 (green). Tumors are marked according to the *CDK12* status: deleterious mutation (X), missense mutation or in-frame indel (+), no mutation (− or no mark for the TCGA cases). E, *CDK12* mutations detected in ovarian cancer cohorts, including nonsense/frameshift (red), splice (green), and missense/in-frame (blue). Mutations associated with the regular gain genomic pattern are shown above the protein outline (plain triangles) and mutations not associated with the pattern are shown below (empty triangles).

It is worth noting that (i) one of the in-house *CDK12*-mutated cases was a low-grade ovarian tumor (supported by 10-year overall survival of the patient without tumor progression); (ii) two cases from the TCGA HGS-OvCa cohort were found with marginally low expression and increased level of *CDK12* promoter methylation; these cases, however, did not display highly altered genomic pattern (Table 1); and (iii) inactivating mutations in *CCNK* (a key partner of CDK12) were not found in the TCGA cohorts (cBioPortal; ref. 13).

Table 1. *CDK12*-related samples from ovarian cancer cohorts

Tumor IDs	WES/RNA-seq	HRD[a]	Ploidy[b]	Breakpoints/iGains[c]	CDK12 TD-plus	*CDK12* mutations
TCGA-09-1673	+/+	No	4	641/70	Yes	p.S343fs
TCGA-13-0791	−/+	No	4	626/64	Yes	p.L122×[d]
TCGA-20-0987	+/+	No	2	491/77	Yes	p.E928Gfs[d]
TCGA-20-1684	+/+	No	4	553/94	Yes	p.S785fs
TCGA-13-0891	−/+	No	4	309/48	Yes	p.Q1013_L1015del
TCGA-24-1842	+/+	No	4	505/68	Yes	p.R983_E984delQ
TCGA-25-1322	+/+	No	2	334/35	Yes	p.Y901C[d]
TCGA-24-1466	+/+	No	4	741/76	Yes	p.L996F[d]
TCGA-31-1953	+/+	No	4	467/38	Yes	p.W719×[d]
TCGA-13-1495	+/+	No	4	409/33	Yes	p.Q602×[d]
TCGA-61-1918	−/+	No	4	498/61	Yes	p.S62fs
TCGA-24-1920	−/−	No	4	846/77	Yes	NA
TCGA-24-2023	−/+	No	4	442/43	Yes	p.S863L
TCGA-42-2588	+/−	No	2	396/41	Yes	Not found
TCGA-24-1551	+/+	No	2	612/85	Yes	c.2964-1G>C
TCGA-61-2000	+/+	Yes	2	521/67	Yes	p.A88fs
TCGA-13-1511	+/+	Yes	2	367/52	Yes	p.P58fs
TCGA-29-1711	+/+	me*BRCA1*	2	166/15	No	p.P653L
TCGA-25-2392	+/+	*BRCA1*	4	212/7	No	p.R882L[e]
TCGA-59-2351	+/+	*BRCA2*	4	94/3	No	p.K975E[f]
TCGA-29-1696	+/+	Yes	2	66/5	No	p.A1174G
TCGA-23-1027	+/+	*BRCA1*	2	73/2	No	p.A943S
TCGA-24-1428	+/+	me*BRCA1*	4	160/5	No	p.A1414T (rs201512860)
TCGA-61-1900	+/+	Yes	2	118/6	No	p.I1131V (rs61747430)
TCGA-09-1665	−/+	me*BRCA1*	4	301/17	No	p.I619V (rs144501352)
TCGA-09-1667	−/+	No	4	200/8	No	Promoter methylation
TCGA-30-1866	−/+	No	4	168/6	No	Promoter methylation
MP2	−/−	Yes	2	394/46	Yes	p.H111Qfs
MP3	−/−	No	4	900/92	Yes	p.E72Gfs
MP4	−/−	Yes	4	717/77	Yes	p.K46Sfs
T_52	−/−	No	2	347/30	Yes	p.V919F
PD3722a	−/−	NA	NA	NA	Yes	p.R271X

[a]*BRCA1*, *BRCA1* deleterious mutation; *BRCA2*, *BRCA2* deleterious mutation; *meBRCA1*, *BRCA1* promoter methylation; yes, genomic HRD identified by the LST signature; no, no evidence of genomic HRD.
[b]Ploidy detected from the SNP arrays (20).
[c]The total number of breakpoints and interstitial gains of 2 to 7 Mb (iGains) are shown.
[d]Pathogenic.
[e]CDK12/CCNK complex not impaired.
[f]CTD phosphorylation not impaired.
[d,e,f]Tested in ref. 8.

Regular gains in *CDK12*-mutated ovarian tumors are due to TDs

Biologic materials from 3 primary ovarian tumors with deleterious *CDK12* mutations from the in-house cohort were investigated by mate-pair WGS (Supplementary Methods). The profiles of structural rearrangements in *CDK12*-inactivated tumors demonstrated overwhelming prevalence of TDs and consistent overlap between the regular gains in the SNP-array profile and the TDs detected by WGS (Fig. 2B; Supplementary Fig. S4; Supplementary Tables S1 and S2).

The lowest number of TDs, 186, was found in MP2 case with a near-diploid genomic content (DNA index = 0.98), where TDs covered 15% of the genome. The near-tetraploid cases MP3 and MP4 (DNA index = 1.78 and 1.92, respectively) had more abundant TDs detected: 797 and 384, with 35% and 30% of the reference genome affected by TDs, respectively. The size distribution of TDs was bimodal with the modes at approximately 0.3 and 3 Mb (Fig. 2C; Supplementary Fig. S5A). It is worth noting that numerous copy-number gains with complex shapes observed in SNP-array profiles mostly corresponded to several TDs affecting a common genomic region (Fig. 2B). When two intersecting TDs are located on the two different alleles, the sizes of TDs reported from mate-pair analysis correspond to the actual sizes of rearrangements. Intersecting TDs on the same allele could give rise to various patterns of copy-number alterations depending on their relative timing and positions. In this context, the size of reported TDs either fits to the actual size or underestimates it (Fig. 2D). Massive appearances of TDs on a near-tetraploid background (four alleles subjected to segmental TDs) form highly altered tumor genomic profiles characteristic of *CDK12* inactivation.

The junction sequences covering the breakpoints (621 split-reads corresponding to ∼45% of all detected TDs) showed overlapping microhomologies with a mode equal to 2 nucleotides ($P < 10^{-15}$, χ^2 test compared with random sampling; Fig. 2E; Supplementary Fig. S5B). Only a small fraction (<4%) of junctions showed the sequence homology in marginal DNA fragments (300 bp were tested using the Blat software and a minimal reported size of 30 bp).

To conclude, mate-pair sequencing showed that the regular gains observed in *CDK12*-inactivated ovarian tumors were almost exclusively due to TDs; TDs are characterized by a bimodal size distribution (with modes at ∼0.3 and ∼3 Mb), displaying overlapping microhomology at the breakpoints (with mode at 2 bp) and showing no significant homology between fragments in the vicinity of the breakpoint junctions.

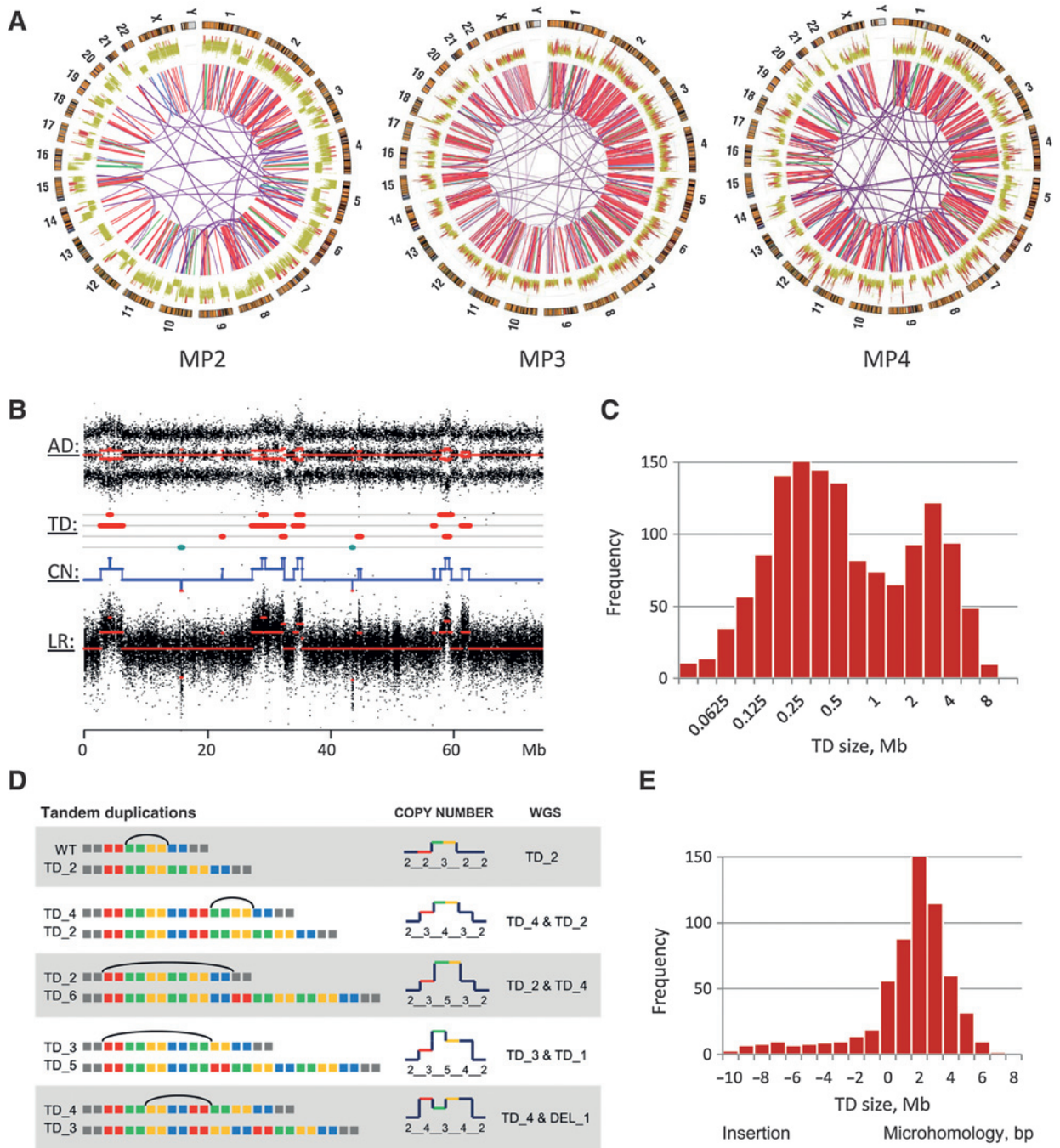

Figure 2.
Whole-genome mate-pair sequencing of 3 *CDK12*-mutated ovarian tumors. A, Circos plots with TDs (red), translocations (violet), deletions (blue), and inversions (green) detected from WGS and largely validated by SNP arrays. B, a fragment of SNP-array profile of chromosome 2p MP2 sample; CN, absolute copy number; LR, log R ratio; AD, allelic difference; TD, tandem duplications (red) and deletions (blue). C, size of TDs summarized for the three sequenced cases. D, intersecting TDs on the same allele (left column) result in different copy-number alteration patterns (middle column) and in some cases are incorrectly attributed from WGS (right column). The symbolic sizes of TD and deletion (DEL) are indicated. E, the size of microhomology at the breakpoint junctions of the TDs summarized for the three sequenced cases.

CDK12-mutated tumors exhibit a peculiar phenotype, designated here as CDK12 TD-plus phenotype

After the description of TDs in one of the first WGS studies of breast cancers (33), two studies specifically addressed TDs in ovarian cancers (15, 16). We reanalyzed publicly accessible data from these studies focusing on *CDK12* and on the size of TDs reported. Two cell lines (PEO14 and PEO23, derived from the same patient at diagnosis and relapse, respectively) described to

have a tandem duplicator phenotype with a high frequency of TDs < 1 Mb (15) did not show any marked rate of interstitial gains of 2 to 7 Mb and were not found mutated in *CDK12* (Fig. 1D; Supplementary Fig. S6). However, the primary tumor PD3722a (16) resembled the *CDK12*-inactivated cases (Supplementary Fig. S7). Amplification of the *CDK12* locus allowed us to discover a nonsense *CDK12* mutation (c.811A>T/p.R271X) in this tumor despite the overall low sequencing coverage. Thus, the frequent TDs described in PD3722a tumor were related to *CDK12* inactivation (16).

In order to clarify the specificity of *CDK12*-inactivated tumors, we analyzed 25 TCGA HGS-OvCa cases with paired-end WGS available. Two tumors displayed the highest TDs rate: TCGA-24-1466 (*CDK12* missense mutation; 346 TDs) and TCGA-13-1487 (*CDK12*-wildtype; 116 TDs; Supplementary Table S3; Supplementary Fig. S8A). The distribution of TD sizes in the *CDK12*-mutated tumor was bimodal, similarly to the in-house cases, whereas a unimodal distribution in the second case yielded >90% of TDs to be <1 Mb (Supplementary Fig. S8B and S8C). It is important to mention that the number of small-size TDs (1–30 kb) did not show any significant increase in the *CDK12*-inactivated case TCGA-24-1466 as compared with the 24 other cases (Supplementary Table S3).

Joint mutational analysis in PEO14/PEO23 cell lines with 10 ovarian and 3 breast cancer cases selected from the TCGA cohorts for accumulation of interstitial gains <1 Mb did not show any recurrent gene impairment explaining the TD phenotype (Supplementary Fig. S9). It is worth noting that among 760 breast tumors, only one case resembled *CDK12*-inactivated tumors but no *CDK12* mutation was found (Supplementary Fig. S10A); in this case, one cannot exclude another inactivating mechanism, such as a translocation involving *CDK12* (34).

We hypothesize that at least two different phenotypes are associated with frequent TDs in a tumor genome: the first one is the TD phenotype consisting of a high rate of TDs <1 Mb and the second one is associated with inactivation of *CDK12* and is characterized by TDs of up to 10 Mb, which could be subsequently designated as TD-plus phenotype (or CDK12 TD-plus phenotype). Besides these phenotypes, TDs are frequent structural alterations observed in many tumor genomes at low/moderate frequencies. The CDK12 TD-plus phenotype occurs at a rate of 3% to 4% in serous ovarian tumors; it consists of hundreds of TDs of up to 10 Mb leading to the duplication of more than 10% of the genome, which is remarkably distinct from what is observed in other ovarian or breast cancer genomes.

Exploring the TCGA cohorts for *CDK12* mutations, we found prostate adenocarcinoma cases with putative biallelic *CDK12* inactivation (cBioPortal; ref. 13). Recurrent *CDK12* mutations were indeed recently reported in advanced prostate cancer (35). Processing 407 SNP arrays from the TCGA prostate adenocarcinoma cohort revealed seven cases (1.7%) with *CDK12* TD-plus phenotype, where *CDK12* inactivation was confirmed in five cases (Supplementary Fig. S10B). Thus, CDK12 TD-plus phenotype is not restricted to the serous ovarian carcinoma, but it also occurs in 1% to 2% of prostate adenocarcinoma.

Stochastic appearance of TDs in CDK12 TD-plus tumors

Genomic localization of TDs could indicate the origin of genomic instability in *CDK12*-mutated tumors, so numerous presumably relevant genomic features were tested for their association to TDs (Supplementary Methods). However, we found overall even distribution of TDs over the human genome, indicating a stochastic character of TD appearance. (i) The GC content at the TDs was similar to the neighboring genome segments as well as to the whole genome (Supplementary Fig. S11A). (ii) Duplicated segments were not found accumulating more somatic mutations compared with the not affected genomic segments (Supplementary Fig. S11B). (iii) TDs did not show any local concentrations or visible heterogeneity within chromosomes (Supplementary Fig. S12). The only TD's enrichment in 3q26 corresponds to the commonly gained region in ovarian carcinomas targeting *MECOM* (1) and is likely to reflect a selection process underlining a probable role of TDs in oncogenesis. (iv) TDs were not found associated to any of tested chromatin structure and organization marks available in the ENCODE project (Supplementary Fig. S13); however, it might be inconclusive in the absence of ovarian cancer cell line profile. (v) Breakpoints in *CDK12*-mutated tumors were not associated with CpG islands and not enriched for any repeated elements. (vi) The position of TD breakpoints was not directly associated with gene or expressed gene loci (~44% breakpoint junctions found inside RefSeq genes did not differed significantly from that of randomly sampled TDs giving 41 ± 1.4%; Supplementary Fig. S14).

In conclusion, duplicated regions in *CDK12*-mutated tumors appear independent from the major genomic features tested, suggesting some general deregulation of the genome maintenance upon *CDK12* inactivation during tumor development.

CDK12 TD-plus phenotype and genomic HRD hallmarks

Effect of *CDK12* knockdown in cellular models has been consistently associated with HRD (3, 5, 7, 8). HRD in breast and ovarian cancers is mostly related to *BRCA1/2* inactivation (9–11). The recently developed genomic signatures of HRD relying on the number of large-scale chromosomal breaks rather efficiently predict *BRCA1/2* inactivation (36). With our discovery of CDK12 TD-plus phenotype, it became clear that genomic instability in *CDK12*-inactivated tumors differs from that of *BRCA1/2*-inactivated tumors. Moreover, the CDK12 TD-plus phenotype in the TCGA cohort is mutually exclusive with *BRCA1/2* mutation (germline or somatic) and with *BRCA1* promoter methylation ($P < 0.001$, Fisher test). To explore whether the genomic profiles of *CDK12*-inactivated tumors carry the footprint of HRD, we evaluated the genomic HRD signatures of these tumors (Supplementary Methods). To be noticed, HRD signatures appeared to be sensitive to TD-plus phenotype, and it was necessary to perform extensive filtering of interstitial gains for consistent predictions (Supplementary Fig. S15). According to the LST signature, TD-plus phenotype could display a genomic HRD (Fig. 3A; Table 1; Supplementary Fig. S16; ref. 9). However, the majority of cases with CDK12 TD-plus phenotype do not reach the threshold for genomic HRD (Fig. 3B). *CDK12*-inactivated tumors resemble the group of non-*BRCA1/2* tumors and mostly (~60%, 13/21) display the number of large-scale alterations (LST number) below the minimal level of *BRCA1/2*-inactivated tumors. Thus, genomic HRD associated with *BRCA1/2* inactivation is not a general feature of the CDK12 TD-plus phenotype.

In addition, ovarian carcinomas with genomic HRD are known to be more sensitive to standard-of-care platinum therapy and to display better overall survival of the patients compared with non-HRD tumors (14, 37). Although in small number, *CDK12*-inactivated tumors did not show any tendency to better overall

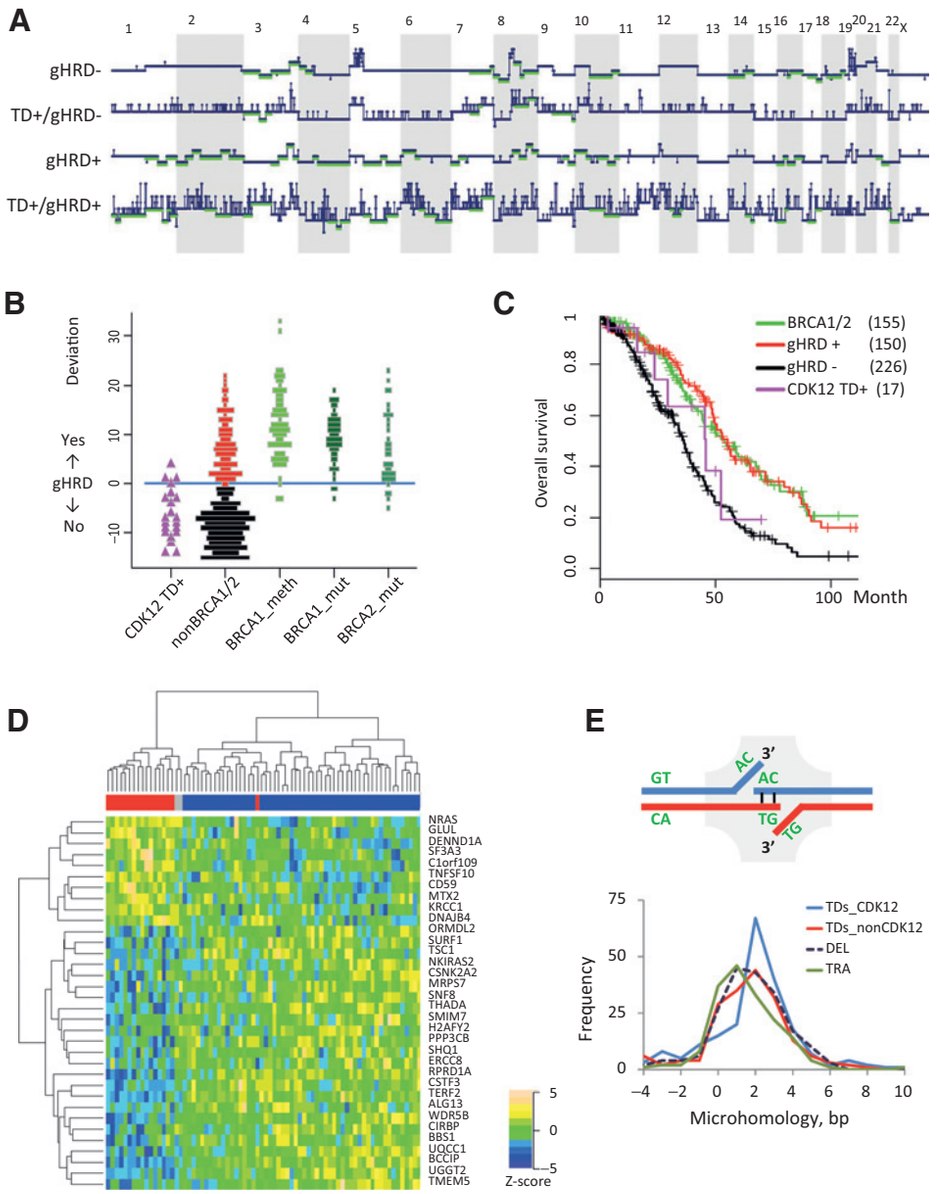

Figure 3.
Comparative analysis of CDK12 TD-plus phenotype. A, examples of tumor copy-number profiles (blue), where the large-scale segments contributing to the LST signature are underlined (green). Profiles are labeled by the phenotype: CDK12 TD-plus (TD+) and/or genomic HRD (gHRD+ or gHRD−) according to the LST signature. B, genomic HRD in ovarian cancers from the TCGA stratified by *BRCA1/2* and *CDK12* statuses. The distance to LST threshold for genomic HRD is shown (*y*-axis): TD-plus phenotype (CDK12 TD+), *BRCA1/2*-mutated (BRCA1_mut and BRCA2_mut), *BRCA1* promoter methylation (BRCA1_meth), and no *BRCA1/2* inactivation found (non-BRCA1/2). C, overall survival for patients from the TCGA ovarian cancer cohort stratified by HRD and *CDK12* statuses: *CDK12* TD-plus phenotype (magenta, $n = 17$), *BRCA1/2*-inactivated (green, $n = 155$), positive gHRD including not sequenced cases (red, $n = 150$), negative gHRD (black, $n = 226$). D, hierarchical clustering built on the top 34 differentially expressed genes (TCGA Affymetrix arrays) in *CDK12* TD-plus tumors (red) versus matched non-*CDK12* cases (blue), including tumors with *CDK12* promoter methylation (gray). E, microhomology size at the breakpoint junctions for TDs in a *CDK12*-mutated context (TDs_CDK12, blue) and TDs (TDs_nonCDK12, red), deletions (DEL, dashed), and translocations (TRA, green) in a *CDK12*-wildtype context (all obtained from 25 TCGA cases with paired-end WGS). A schema of microhomology arisen at the end's joining is shown above.

survival compared with ovarian cancers without genomic HRD ($P > 0.3$, log-rank test; Fig. 3C).

To conclude, genomic instability in *CDK12*-inactivated ovarian tumors is clearly different from the genomic HRD associated with *BRCA1/2* inactivation. However, only direct evaluation of the HR pathway in cancer cell lines (or tumor samples) with *CDK12* deleterious mutations will allow definitive conclusion about the status of the HR pathway.

Comparative transcriptomic analysis of *CDK12*-inactivated ovarian tumors

Having defined tumors with the CDK12 TD-plus phenotype, we performed transcriptomic analysis in order to find genes and/or pathways affected by *CDK12* inactivation. We first explored the molecular features of *CDK12*-inactivated tumors in order to minimize confounding factors in the context of highly heterogeneous HGS-OvCa cohort. Analysis of four molecular subtypes defined in HGS-OvCa (mesenchymal, proliferative, immunoreactive, differentiated; ref. 1) showed that tumors with CDK12 TD-plus phenotype do not cluster with the mesenchymal subtype ($P < 0.02$, Fisher test; Supplementary Fig. S17). Tumors with CDK12 TD-plus phenotype were not found inactivated for *BRCA1/2* (as already mentioned above) or *CDKN2A* (found in 27% of non-mesenchymal HGS-OvCa, $P < 0.01$, Fisher test) and mostly expressed high level of *CCNE1* (Supplementary Fig. S18A). Differential analysis of 17 CDK12 TD-plus tumors versus 57 matched cases from the reference group (see Material and Methods) showed 222 differentially expressed genes ($P < 0.01$, ~25% false discovery rate; Supplementary Fig. S18B; see Supplementary Table S4 for the gene list). Sample clustering based on the top 34

deregulated genes ($P < 0.001$ and absolute log fold change > 1) supported the association of the gene list with *CDK12* inactivation: 2 *CDK12* methylated cases (without TD-plus phenotype and included in the reference group) clustered together with *CDK12*-mutated cases, whereas only one case with TD-plus phenotype and without *CDK12* mutation did not (Fig. 3D). These results were largely consistent between platforms (RNA-seq and Affymetrix) and between cohorts (TCGA and in-house; Supplementary Fig. S18C). However, pathway analysis did not show any significant enrichment. In contrast with *CCNK*/*CDK12* knockdown experiments, large genes were not markedly abundant among the downregulated ones; *TERF2*, *FANCI*, *ORC3*, and *ERCC1* were the only intersection with DNA repair genes mentioned in refs. 3, 5. From the other hand, significant enrichment in large genes was observed for the set of genes positively correlated to *CDK12* ($P < 10^{-15}$, *t* test, TCGA RNA-seq; Supplementary Fig. S19). For example, *ATM* showed a moderate correlation to *CDK12*, and its marginal relative downregulation in *CDK12*-inactivated cases could be observed ($P < 0.02$; Supplementary Fig. S20). To be noticed, *ATM* also had a decreased expression in the three *CDK12*-inactivated cases from the in-house cohort (fold change > 2; $P > 0.05$).

The absence of pathway enrichment in expression analysis could be partially explained by the significant input from the differential copy-number alterations: 25% to 30% of differentially expressed genes followed the direction of change in relative copy numbers ($P < 0.05$, *t* test; Supplementary Table S4). The only one exception displaying downregulation and significantly higher relative-copy number in *CDK12*-inactivated tumors is *CSTF3* (3′ pre-RNA cleavage stimulation factor, chr11p13). CSTF3 has direct functional connection with CDK12 being involved in the 3′ end formation of pre-mRNA, a process coupled with CDK12-dependent Ser2 CTD phosphorylation (38). The top downregulated gene in *CDK12*-mutated tumors, validated in all cohorts, is *RPRD1A* (Regulation of Nuclear Pre-mRNA Domain Containing 1A), which interacts with phosphorylated CTD of the RNA pol II and participates in dephosphorylation of the CTD (39). Consistent downregulation of *CSTF3* and *RPRD1A* may evidence a compensatory mechanism developed by tumors upon *CDK12* inactivation, which would explain the different gene sets obtained in tumors and cellular models.

Microhomology end joining pattern as compared with *CDK12*-wildtype tumors

Microhomology at the breakpoint junctions of structural genomic rearrangements is a rather common phenomenon (40). Our analysis based on the 25 WGS cases from the TCGA HGS-OvCa cohort demonstrated that microhomology detected at the breakpoint junctions of TDs in the CDK12 TD-plus phenotype was in general similar to that found in TDs, translocations, and deletions in *CDK12*-wildtype ovarian tumors (Fig. 3E; Supplementary Table S3). However, microhomology size distribution in CDK12 TD-plus phenotype tumors showed significant difference from that in other structural alterations due to a more pronounced peak at 2 bp ($P < 0.0014$, χ^2 test).

Small overlapping microhomology at the TD breakpoint junctions in SKOV3 cell line (mate-pair WGS) displayed feeble bimodality with the most frequent microhomology being at 1 bp overlap, which also differed significantly from *CDK12*-mutated tumors (Supplementary Figs. S21 and S22).

Altogether, the abnormal junctions in ovarian tumors were found to have overall similar features, whether they arose from large or small TDs or from translocations and deletions; the results are concordant with those obtained previously (33).

It is not clear which pathway is employed for TD resolutions, as both nonhomologous end joining frequently operating with 1 to 4 bp microhomology (41) and microhomology-mediated end joining utilizing longer 5 to 25 bp stretches of homologous fragments are consistent with the observed microhomology size distribution (40).

Discussion

Here, we reported a new genomic instability pattern consisting of a high number of TDs up to 10 Mb in size and associated it with inactivation of *CDK12* gene. Three ovarian tumors mutated in *CDK12* that were investigated by mate-pair WGS exhibited 200 to 800 TDs per tumor; these TDs were quasi-randomly distributed along the genomes and affected more than 10% of the genomic content. This genomic instability phenotype was denoted here as the CDK12 TD-plus phenotype. The CDK12 TD-plus phenotype was observed in around 4% of serous ovarian carcinomas and in 1% to 2% of prostate adenocarcinomas. Analysis of more than 1,000 breast cancers identified only one case resembling the TD-plus phenotype, which was not found mutated for *CDK12*.

This novel genomic instability observed in *CDK12*-inactivated ovarian and prostate cancers is the first described connection between massive genomic TDs and gene impairment in tumors. This finding gives a new perspective on the gene function and has direct connection to clinical application. The outstanding questions emerging from our study are which biologic mechanisms are responsible for the TDs formation and how impaired *CDK12* leads to these genomic defects.

Analysis of a number of particular genomic features within and around TDs in the *CDK12*-mutated context gave no preference for TDs localization evidencing some general deregulation and stochastic process. The overwhelming prevalence of gains versus losses and absence of homologous fragments around the breakpoints excluded any "symmetric" mechanisms, such as misalignment of the sister chromatids or unbalanced translocations. Two processes leading to TDs have been described so far: DNA re-replication due to origin re-firing (42) or break-induced replication (BIR) associated to the strand invasion (43). The sizes of TDs resulted from BIR activated by cyclin E (*CCNE1*)–induced replication stress were measured to be hundreds of kb with the median around 200 kb and importantly, near one third of reported alterations were deletions (44). An increased rate of DNA double-strand breaks and release of DNA fragments consecutive to re-replicating fork collisions were shown in model systems of induced re-replication (45, 46). Resolution of these breaks could result in TDs (42). CDK12 TD-plus phenotype seems unlikely to be due to a BIR process, as the proportion of deletions in a *CDK12*-null context is much smaller than in the BIR-induced system. The re-replication hypothesis would seem more likely but does not account for the megabase size of *CDK12*-related TDs. The sizes of TDs are close to the size of the replication domains, which is too large to be replicated from the re-fired single origin and could suggest the re-initialization in the whole replication domains. This process has never been described in cellular models, whether yeast or mammalian.

The roles and consequences of *CDK12* inactivation in ovarian cancers were previously addressed in several studies. DNA repair impairment and PARP inhibitor hypersensitivity observed upon *CDK12* knockdown were explained by the indirect role of CDK12 affecting the transcription of key factors of the HR pathway (5, 6, 8). We addressed the *CDK12* and HR connection by looking at the genomic footprint of HRD. Genomic HRD (as defined by the genomic signature) was found in approximately 50% of serous ovarian cancers and beside *BRCA1/2* was linked only to *RAD51C* inactivation (11). We show here that after filtering interstitial gains, *CDK12*-inactivated tumors mostly display less large-scale chromosomal breaks than *BRCA1/2*-inactivated ovarian cancers. Thus, genomic instability associated with *CDK12* inactivation does not display substantial genomic HRD in addition to massive TDs.

This raises further questions such as: does HR downregulation observed in cellular models upon *CDK12* knockdown represent the major effect of *CDK12* inactivation in tumors causing TD-plus phenotype (for example, TDs are shown to be abundant in HCC38 *BRCA1* methylated cell line; ref. 33); or are there alternative/additional targets of *CDK12* inactivation affecting genomic integrity? In depth, transcriptomic analyses did not show any candidate gene to explain the phenotype, but identified possible compensatory mechanisms (downregulation of *CSTF3* and *RPRD1A*) that could have rescued gene expression changes since *CDK12* inactivation.

Beside the role of *CDK12* on gene expression, one could hypothesize that sudden *CDK12* inactivation may cause transcription stalling, which may interfere with replication forks, generating the observed TDs. However, this hypothesis was not supported by our analyses. The majority of TDs exceeded in size the transcribed sequences, and no correlation between TD positions and gene loci was observed. Nevertheless, the general role of transcriptional stress on TD formation (due to BIR or re-replication) could not be excluded, and relationship between transcriptional stress and HR has recently been established (47).

Another intriguing observation is the two ovarian cancers found to have a total silencing of *CDK12* by promoter methylation with concordant transcriptomic change and without TD-plus phenotype. The timing of *CDK12* inactivation in the transformation process could be a critical parameter for the onset of genomic instability.

To conclude, our finding of a CDK12 TD-plus phenotype poses many direct questions and opens a new perspective in deciphering *CDK12* function, its role in oncogenesis, and genomic instability, and the recently established analogue-sensitive CDK12 cell line will be instrumental in this regard (48).

Disclosure of Potential Conflicts of Interest

T. Popova has expert testimony in patent licensed to Myriad Genetics. E. Manié reports receiving other commercial research support from Myriad Genetics. M.-H. Stern reports receiving other commercial research support from Myriad Genetics. No potential conflicts of interest were disclosed by the other authors

Authors' Contributions

Conception and design: T. Popova, X. Sastre-Garau, M.-H. Stern
Development of methodology: T. Popova
Acquisition of data (provided animals, acquired and managed patients, provided facilities, etc.): E. Manié, N.K. Smith, O. Mariani, X. Sastre-Garau
Analysis and interpretation of data (e.g., statistical analysis, biostatistics, computational analysis): T. Popova, E. Manié, V. Boeva, N.K. Smith, C.R. Mueller
Writing, review, and/or revision of the manuscript: T. Popova, E. Manié, V. Boeva, C.R. Mueller, M.-H. Stern
Administrative, technical, or material support (i.e., reporting or organizing data, constructing databases): A. Battistella, O. Goundiam, V. Raynal, O. Mariani
Study supervision: T. Popova, M.-H. Stern

Acknowledgments

The authors thank Andrey Zinovyev, Benoit Le Tallec, Sarah Lambert, Arturo Londono, Alain Nicolas, Michèle Debatisse, Sophie Loeillet, Chunlong Chen, and Olivier Bensaude for helpful discussions and/or critical readings of the draft.

Grant Support

This study was supported by Institut National de la Santé et de la Recherche Médicale, Cancéropôle Ile-de-France, INCa, Institut Curie and its Translational Research Department. A. Battistella is supported by a grant from INCa.

The costs of publication of this article were defrayed in part by the payment of page charges. This article must therefore be hereby marked *advertisement* in accordance with 18 U.S.C. Section 1734 solely to indicate this fact.

Received August 3, 2015; revised January 7, 2016; accepted January 8, 2016; published OnlineFirst January 19, 2016.

References

1. Cancer Genome Atlas Research N. Integrated genomic analyses of ovarian carcinoma. Nature 2011;474:609–15.
2. Chen HH, Wang YC, Fann MJ. Identification and characterization of the CDK12/cyclin L1 complex involved in alternative splicing regulation. Mol Cell Biol 2006;26:2736–45.
3. Blazek D, Kohoutek J, Bartholomeeusen K, Johansen E, Hulinkova P, Luo Z, et al. The Cyclin K/Cdk12 complex maintains genomic stability via regulation of expression of DNA damage response genes. Genes Dev 2011;25:2158–72.
4. Liang K, Gao X, Gilmore JM, Florens L, Washburn MP, Smith E, et al. Characterization of human cyclin-dependent kinase 12 (CDK12) and CDK13 complexes in C-terminal domain phosphorylation, gene transcription, and RNA processing. Mol Cell Biol 2015;35:928–38.
5. Joshi PM, Sutor SL, Huntoon CJ, Karnitz LM. Ovarian cancer-associated mutations disable catalytic activity of CDK12, a kinase that promotes homologous recombination repair and resistance to cisplatin and poly(ADP-ribose) polymerase inhibitors. J Biol Chem 2014;289:9247–53.
6. Bajrami I, Frankum JR, Konde A, Miller RE, Rehman FL, Brough R, et al. Genome-wide profiling of genetic synthetic lethality identifies CDK12 as a novel determinant of PARP1/2 inhibitor sensitivity. Cancer Res 2014;74:287–97.
7. Cheng SW, Kuzyk MA, Moradian A, Ichu TA, Chang VC, Tien JF, et al. Interaction of cyclin-dependent kinase 12/CrkRS with cyclin K1 is required for the phosphorylation of the C-terminal domain of RNA polymerase II. Mol Cell Biol 2012;32:4691–704.
8. Ekumi KM, Paculova H, Lenasi T, Pospichalova V, Bosken CA, Rybarikova J, et al. Ovarian carcinoma CDK12 mutations misregulate expression of DNA repair genes via deficient formation and function of the Cdk12/CycK complex. Nucleic Acids Res 2015;43:2575–89.
9. Popova T, Manie E, Rieunier G, Caux-Moncoutier V, Tirapo C, Dubois T, et al. Ploidy and large-scale genomic instability consistently identify basal-like breast carcinomas with BRCA1/2 inactivation. Cancer Res 2012;72:5454–62.

10. Birkbak NJ, Wang ZC, Kim JY, Eklund AC, Li Q, Tian R, et al. Telomeric allelic imbalance indicates defective DNA repair and sensitivity to DNA-damaging agents. Cancer Discov 2012;2:366–75.
11. Abkevich V, Timms KM, Hennessy BT, Potter J, Carey MS, Meyer LA, et al. Patterns of genomic loss of heterozygosity predict homologous recombination repair defects in epithelial ovarian cancer. Br J Cancer 2012;107:1776–82.
12. The Cancer Genome Atlas http://cancergenome.nih.gov. Accessed 20 May 2015.
13. cBioPortal for cancer genomics http://cbioportal.org/. Accessed 20 May 2015.
14. Goundiam O, Gestraud P, Popova T, De la Motte Rouge T, Fourchotte V, Gentien D, et al. Histo-genomic stratification reveals the frequent amplification/overexpression of CCNE1 and BRD4 genes in non-BRCAness high grade ovarian carcinoma. Int J Cancer 2015;137:1890–900.
15. Ng CK, Cooke SL, Howe K, Newman S, Xian J, Temple J, et al. The role of tandem duplicator phenotype in tumour evolution in high-grade serous ovarian cancer. J Pathol 2012;226:703–12.
16. McBride DJ, Etemadmoghadam D, Cooke SL, Alsop K, George J, Butler A, et al. Tandem duplication of chromosomal segments is common in ovarian and breast cancer genomes. J Pathol 2012;227:446–55.
17. Barretina J, Caponigro G, Stransky N, Venkatesan K, Margolin AA, Kim S, et al. The Cancer Cell Line Encyclopedia enables predictive modelling of anticancer drug sensitivity. Nature 2012;483:603–7.
18. Affymetrix www.affymetrix.com. Accessed 20 May 2015.
19. Illumina www.illumina.com. Accessed 20 May 2015.
20. Popova T, Manie E, Stoppa-Lyonnet D, Rigaill G, Barillot E, Stern MH. Genome Alteration Print (GAP): a tool to visualize and mine complex cancer genomic profiles obtained by SNP arrays. Genome Biol 2009;10:R128.
21. Homer N, Merriman B, Nelson SF. BFAST: an alignment tool for large scale genome resequencing. PLoS One 2009;4:e7767.
22. Li H, Durbin R. Fast and accurate short read alignment with Burrows-Wheeler transform. Bioinformatics 2009;25:1754–60.
23. Li H, Handsaker B, Wysoker A, Fennell T, Ruan J, Homer N, et al. The sequence alignment/map format and SAMtools. Bioinformatics 2009;25:2078–9.
24. Quinlan AR, Hall IM. BEDTools: a flexible suite of utilities for comparing genomic features. Bioinformatics 2010;26:841–2.
25. Picard http://broadinstitute.github.io/picard/. Accessed 20 May 2015.
26. Robinson JT, Thorvaldsdottir H, Winckler W, Guttman M, Lander ES, Getz G, et al. Integrative genomics viewer. Nat Biotechnol 2011;29:24–6.
27. Zeitouni B, Boeva V, Janoueix-Lerosey I, Loeillet S, Legoix-ne P, Nicolas A, et al. SVDetect: a tool to identify genomic structural variations from paired-end and mate-pair sequencing data. Bioinformatics 2010;26:1895–6.
28. Rausch T, Zichner T, Schlattl A, Stutz AM, Benes V, Korbel JO. DELLY: structural variant discovery by integrated paired-end and split-read analysis. Bioinformatics 2012;28:i333–i39.
29. Boeva V, Popova T, Bleakley K, Chiche P, Cappo J, Schleiermacher G, et al. Control-FREEC: a tool for assessing copy number and allelic content using next-generation sequencing data. Bioinformatics 2012;28:423–5.
30. Krzywinski M, Schein J, Birol I, Connors J, Gascoyne R, Horsman D, et al. Circos: an information aesthetic for comparative genomics. Genome Res 2009;19:1639–45.
31. Wang K, Li M, Hakonarson H. ANNOVAR: functional annotation of genetic variants from high-throughput sequencing data. Nucleic Acids Res 2010;38:e164.
32. *R* Development Core Team. *R*: A language and environment for statistical computing. Vienna, Austria: R Foundation for Statistical Computing, 2011.
33. Stephens PJ, McBride DJ, Lin ML, Varela I, Pleasance ED, Simpson JT, et al. Complex landscapes of somatic rearrangement in human breast cancer genomes. Nature 2009;462:1005–10.
34. Natrajan R, Wilkerson PM, Marchio C, Piscuoglio S, Ng CK, Wai P, et al. Characterization of the genomic features and expressed fusion genes in micropapillary carcinomas of the breast. J Pathol 2014;232:553–65.
35. Robinson D, VanAllen EM, Wu YM, Schultz N, Lonigro RJ, Mosquera JM, et al. Integrative clinical genomics of advanced prostate cancer. Cell 2015;161:1215–28.
36. Timms KM, Abkevich V, Hughes E, Neff C, Reid J, Morris B, et al. Association of BRCA1/2 defects with genomic scores predictive of DNA damage repair deficiency among breast cancer subtypes. Breast Cancer Res 2014;16:475.
37. Mukhopadhyay A, Plummer ER, Elattar A, Soohoo S, Uzir B, Quinn JE, et al. Clinicopathological features of homologous recombination-deficient epithelial ovarian cancers: sensitivity to PARP inhibitors, platinum, and survival. Cancer Res 2012;72:5675–82.
38. Davidson L, Muniz L, West S. 3′ end formation of pre-mRNA and phosphorylation of Ser2 on the RNA polymerase II CTD are reciprocally coupled in human cells. Genes Dev 2014;28:342–56.
39. Ni Z, Olsen JB, Guo X, Zhong G, Ruan ED, Marcon E, et al. Control of the RNA polymerase II phosphorylation state in promoter regions by CTD interaction domain-containing proteins RPRD1A and RPRD1B. Transcription 2011;2:237–42.
40. Ottaviani D, LeCain M, Sheer D. The role of microhomology in genomic structural variation. Trends Genet 2014;30:85–94.
41. Pannunzio NR, Li S, Watanabe G, Lieber MR. Non-homologous end joining often uses microhomology: implications for alternative end joining. DNA Repair (Amst) 2014;17:74–80.
42. Blow JJ, Gillespie PJ. Replication licensing and cancer–a fatal entanglement? Nat Rev Cancer 2008;8:799–806.
43. Llorente B, Smith CE, Symington LS. Break-induced replication: what is it and what is it for? Cell Cycle 2008;7:859–64.
44. Costantino L, Sotiriou SK, Rantala JK, Magin S, Mladenov E, Helleday T, et al. Break-induced replication repair of damaged forks induces genomic duplications in human cells. Science 2014;343:88–91.
45. Davidson IF, Li A, Blow JJ. Deregulated replication licensing causes DNA fragmentation consistent with head-to-tail fork collision. Mol Cell 2006;24:433–43.
46. Neelsen KJ, Zanini IM, Mijic S, Herrador R, Zellweger R, Ray Chaudhuri A, et al. Deregulated origin licensing leads to chromosomal breaks by rereplication of a gapped DNA template. Genes Dev 2013;27:2537–42.
47. Hatchi E, Skourti-Stathaki K, Ventz S, Pinello L, Yen A, Kamieniarz-Gdula K, et al. BRCA1 recruitment to transcriptional pause sites is required for R-loop-driven DNA damage repair. Mol Cell 2015;57:636–47.
48. Bartkowiak B, Yan C, Greenleaf AL. Engineering an analog-sensitive CDK12 cell line using CRISPR/Cas. Biochim Biophys Acta 2015;1849:1179–87.